

Competitive Adsorption of $\text{La}^{3+}/\text{Ce}^{3+}/\text{Nd}^{3+}$ Ions on Poly(Methyl Methacrylate)-co-Diacrylate/Single-Walled Carbon Nanotube Nanocomposites

Nurul Jamilah^{1,2}, Asep Riswoko³, Adam Badra Cahaya^{1,*}

¹Department of Physics, Faculty of Mathematics and Natural Sciences, University of Indonesia, Depok, West Java, Indonesia

²Research Center for Polymer Technology, National Research and Innovation Agency (BRIN), South Tangerang, Banten, Indonesia

³Directorate of Research and Innovation Partnerships, National Research and Innovation Agency (BRIN), Central Jakarta, Jakarta, Indonesia

*Author to whom correspondence should be addressed:

E-mail: adam@sci.ui.ac.id

(Received October 29, 2024; Revised June 07, 2025; Accepted July 02, 2025)

Abstract: Recovery of rare earth elements (REEs) is one of the important processes in high-end industries using critical raw materials. In this study, we developed a new microencapsulated nanocomposite adsorbent consisting of poly(methyl methacrylate) copolymerized with liquid crystal diacrylate (RM 257) and single-walled carbon nanotube (SWCNT). The adsorbent was synthesized by oil-in-water (O/W) emulsion polymerization with the ratio 1:7 and aimed to recover La^{3+} , Ce^{3+} , and Nd^{3+} ions in an aqueous solution. The FTIR and Raman spectroscopy results confirm the components that formulate this microencapsulation. Besides that, FTIR, BET, and SEM-EDS have characterized the microencapsulated adsorbents before and after adsorption. The morphology and element mapping using SEM-EDS showed that Ce^{3+} and Nd^{3+} ions are distributed well on the surface of the adsorbent, whereas La^{3+} diffused into the pores of the adsorbent. The kinetics and isotherm models have been fitted to evaluate the competitive adsorption of $\text{La}/\text{Ce}/\text{Nd}$ ions at low concentrations (0.5–6 mg/L). The study found that the adsorption of La^{3+} , Ce^{3+} , and Nd^{3+} ions in an aqueous solution followed pseudo-second-order kinetics and the Freundlich isotherm model. The maximum adsorption capacity was 0.1538, 0.1352, and 0.1217 mg/g for La^{3+} , Nd^{3+} , and Ce^{3+} ions.

Keywords: adsorption; carbon nanotube; microencapsulation; nanocomposite; rare earth elements

1. Introduction

Lanthanum (La), cerium (Ce), and neodymium (Nd) are classified as rare earth elements (REEs) and are becoming increasingly crucial to high-tech and renewable energy sectors. According to Kusriani et al., REEs are important in modern technology for the military, energy, health care, and economic sectors¹. Similarly, Balaram states that these metals are now essential to modern technology, from smartphones and televisions to LED lightbulbs and wind turbines². In addition, they play a vital role in the electronics industry, energy storage and conversion, and the electric vehicle industry. One of them, neodymium, is primarily used in permanent magnets for wind turbines and electric motors in electric vehicles³. Indonesia has an enormous potential for rare earth

elements (REEs), especially in the tin-related monazite mineral. According to Setiawan, the Bangka Islands are the primary source of REE from the remaining tin mining process and are associated with radioactive minerals such as monazite and xenotime, which are difficult to extract and contain high radioactivity⁴. Therefore, because this mineral is a by-product, a secondary output from a process considered uneconomical for further separation due to the high processing costs, it ends up as landfill material. In addition, electronic waste (e.g., computers, liquid-crystal display (LCD) screens, and smartphones), which contains a lot of valuable metals, one of which is REEs, is experiencing a continuous increase. According to Mairizal et al., the estimate of this stockpile will reach around 10 kg/capita in 2040, equivalent to an economic value of US\$ 14 billion in copper, gold, silver, platinum, and

palladium⁵). Both have great potential, which necessitates the development of effective methods for their separation and recovery.

Rare earth element (REE) separation often involves the use of traditional extraction techniques, such as liquid-liquid extraction (LLE), as opposed to solid-phase extraction (SPE), which is less cost-effective and ecologically benign. This is due to the use of high levels of chemicals, high operational costs, and low purity of the extracted elements. Liu and Chen state that solvent extraction can provide high selectivity, a good separation effect, and a large processing capacity. However, the disadvantages are using organic solvents that are harmful to the environment, the long process requiring more steps, and the massive consumption of extractants to obtain high purity⁶). Similarly, Merroune et al. reviewed that solvent extraction in the LLE method is widely recognized as the primary industrial process for REE extraction but is limited by impurity handling and the need for advanced separation techniques to achieve high yields and purity of the final REE products⁷).

In contrast, the solid-phase extraction (SPE) method, such as adsorption, has shown significant advantages. According to Asadollahzadeh et al., adsorption is a feasible and reliable economic process for removing and recovering rare earth elements (REEs) from aqueous solutions or wastewater because adsorption can be enhanced by various innovations in the production of suitable adsorbents, the adsorption process is flexible in design and operation, can be used multiple times using suitable adsorbents, and can be recycled in a reversible process⁸). Cardoso et al. state that enhanced extractant-REE interaction in the water phase and a large surface area are two benefits of the SPE approach⁹). These two benefits can lower chemical consumption by improving extraction efficiency, selectivity, quality, and contact area. One of the research results of Hu et al., who developed mesoporous silica functionalized by preorganized chelating ligands, showed high efficiency and selectivity in REE inspection, with significant adsorption capacity and good regeneration ability¹⁰). Compared to other methods, this one also requires less maintenance, is easier to install and run, and has a high release/desorption efficiency, as outlined by Jamilah et al.¹¹). However, according to Xuyi et al., the adsorption capacity using mineral-, carbon-, and polymer-based adsorbents depends on operating conditions such as pH, contact time, and ion concentration¹²). In this new technological era, mining, stockpiling, and refining processes release large amounts of toxic liquid waste and sludge into the environment because of the growing demand for REEs. Therefore, developing an optimization process and an environmentally friendly method for recovering REEs is essential. One of the latest breakthroughs in environmentally friendly adsorption methods is the application of micro-encapsulated

nanocomposite adsorbents based on carbon nanotubes (CNTs) for fixed-bed adsorption in SPE.

Several studies have shown that nanocomposite adsorbents effectively separate and recover rare earth elements (REEs). Some advantages of nanocomposites as adsorbents are their porous structure with a high surface area, surface functionalization, outstanding regeneration ability, and good thermal and chemical stability. This is based on the studies by Unsworth et al., who developed an adsorbent from DNA-functionalized mesoporous carbon with a high surface area, showing higher REE adsorption results than pure mesoporous carbon¹³). Similarly, Jamilah et al. created a polymer-based composite adsorbent modified with carbon nanotubes, which showed high adsorption efficiency for REE ions at pH 4 and a contact time of 90 min¹⁴). In addition, Wei et al. developed a novel adsorbent, PEI-ALG@KLN, synthesized through surface modification of kaolinite-alginate hydrogel with polyethyleneimine, which showed good regeneration ability (adsorption efficiency > 85% after 5 adsorption-desorption cycles), capable of efficiently and selectively adsorbing REE from wastewater¹⁵). Additionally, Al-Salem et al. reported the performance of magnetic chitosan@graphene oxide (MCh@GO) composites, which have thermal stability and have proven to be excellent adsorbents for Nd purification, remediation, and separation¹⁶). Therefore, nanocomposite adsorbents are the right choice for application in REE recovery.

Carbon nanotubes (CNTs) are generally irregular or powder-shaped adsorbent materials. Powdered and irregular adsorbents require a complex separation process because the adsorbent is dispersed in water media, so the filtering process uses a filter with a small pore size. However, with the microencapsulation method, this CNT-based adsorbent can be in granular or bead form, making it easier to adsorb and reusable.

Based on their structural form, carbon nanotubes (CNTs) are divided into two types, namely single-walled carbon nanotubes (SWCNTs) and multi-walled carbon nanotubes (MWCNTs). Both have different characteristics according to the application used. Some fundamental differences between the two types of CNTs include physical properties such as surface area and internal diameter size, chemical properties such as surface modification and reactivity, and mechanical properties such as mechanical stability. According to Birch et al., the specific surface area of SWCNT (600-1300 m²/g) is higher than MWCNT (400-1000 m²/g)¹⁷). Meanwhile, according to Sonkar et al., the internal diameter of SWCNT (0.2-2 nm) is lower than MWCNT (1-3 nm)¹⁸). According to Ménard-Moyon et al., the surface of SWCNT is more reactive than MWCNT, so it is easy to functionalize¹⁹). However, the disadvantage of SWCNT is lower mechanical stability. The research results from Monthieux et al. showed changes in the SWNT structure due to acid purification, soaking in

dimethylformamide (DMF), and increasing temperature, resulting in SWNT degradation (complete amorphization)²⁰. Another disadvantage of SWCNTs, according to Nag et al., is the higher production cost than MWCNTs because, from a fabrication point of view, mass formation of MWCNTs is easier, accompanied by increased electrical, thermal, and chemical stability²¹.

Microencapsulation methods, according to Fadilah et al., involve the physical packaging of active material (core material), such as solid particles, water droplets, or gasses, in the form of thin-film layers within secondary materials (walls)²². According to Ahangaran et al., the shell or wall material in encapsulation that is widely used is poly(methyl methacrylate) (PMMA) because of its high chemical stability, biocompatibility, non-toxicity, and good mechanical properties²³. The microencapsulated or bead structure is produced through an emulsion polymerization process involving surfactants and polymerization initiators, followed by a solvent evaporation step. The evaporation process results in a porous and granular structure, which enhances the material's adsorption capacity. With this new application, microencapsulated adsorbents are promising candidates for REE ion adsorption.

In this study, methyl methacrylate (MMA) and reactive mesogen diacrylate (RM257) were used as the matrix and secondary materials, with octadecyl amine functionalized single-walled carbon nanotubes (ODA-SWCNTs), which serve as reinforcement and active material. We use ODA-SWCNT because, based on its characteristics, it is more suitable than multi-walled carbon nanotubes (MWCNT), both in the adsorbent fabrication process using microencapsulation with acrylate monomers and in the adsorption involving adsorbates of rare earth elements (REEs). The superior characteristics of SWCNT, including the specific surface area of SWCNT around 600-1300 m²/g¹⁷, facilitate metal adsorption so that it can increase adsorption capacity and has an internal diameter of around 0.2-2 nm¹⁸, facilitate selective adsorption of small REE ions (0.95-1.05 Å)²⁴. Its surface is more reactive for functionalization, such as using octadecyl amine (ODA-SWCNT) for more microencapsulation with acrylate monomers¹⁹. The resulting nanocomposite material, composed of poly(methyl methacrylate)-co-diacrylate/SWCNT, is expected to exhibit valuable properties such as high chemical stability, biocompatibility, non-toxicity, and favourable mechanical characteristics, including a high Young's modulus and low elongation at break.

In this research, an experiment was conducted on the adsorption of rare earth element (REE) ions, especially lanthanum (La³⁺), cerium (Ce³⁺), and neodymium (Nd³⁺), in a simulated standard mixed aqueous solution of REE ions at low concentration using poly(methyl methacrylate)-co-diacrylate/SWCNT nanocomposite

adsorbent microcapsules. The recovery performance of a microencapsulated adsorbent of poly(methyl methacrylate)-co-diacrylate/SWCNT nanocomposite on a mixture of La³⁺, Ce³⁺, and Nd³⁺ ions in aqueous solution was observed and evaluated. The kinetics and adsorption capacities of La³⁺, Ce³⁺, and Nd³⁺ ions were examined.

2. Materials and methods

2.1. Chemicals

2-Methyl-1,4-phenylene bis(4-(3-(acryloyloxy) propoxy) benzoate) or reactive mesogen diacrylate (RM257) was purchased from Daken Chemical, China. Octadecyl amine functionalized single-walled carbon nanotubes (ODA-SWCNT), benzoyl peroxide (BPO) as an initiator of polymerization, polyvinyl pyrrolidone (PVP) as a surfactant, and methyl methacrylate (MMA) as a solvent for microencapsulation were purchased from Sigma-Aldrich Co., Ltd., Germany. The entire trial was conducted with distilled water.

2.2. Preparation of Microencapsulated Nanocomposite

Microencapsulation of the poly(methyl methacrylate)-co-diacrylate/SWCNT nanocomposite was conducted using the emulsion polymerization of oil in water (O/W) with the flowchart diagram seen in Figure 1.

The ratio of oil to water was 1:7. The oil phase used was a mixture of reactive mesogen diacrylate (RM257) (2 g) and Octadecyl amine functionalized single-walled carbon nanotubes (ODA-SWCNT) (0.01 g) dissolved in methyl methacrylate (MMA) (20 mL) using ultrasonics at 130 W for around 18 minutes in an ice water bath to prevent a temperature rise²⁵, while the water phase used was distilled water containing 1.5% polyvinyl pyrrolidone (PVP) from the water phase as a surfactant²⁶⁻²⁸. The oil phase was added dropwise to the water phase in an ice

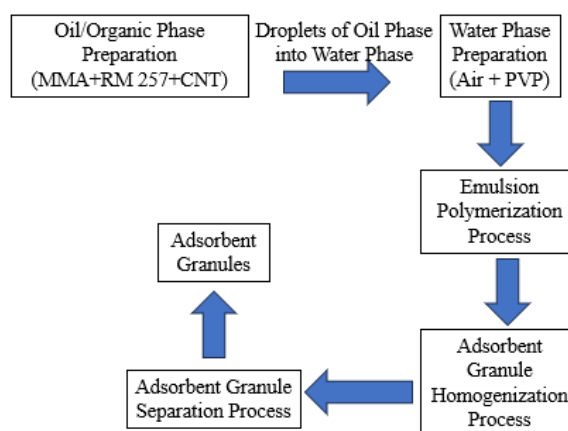


Fig. 1: Flowchart of adsorbent microencapsulation of the poly(methyl methacrylate)-co-diacrylate/SWCNT nanocomposite

water bath to prevent microencapsulated damage because of temperature increases, and the stirrer was about 200 rpm to make an oil-in-water (O/W) emulsion²⁵. After an O/W emulsion formed, the mixture was radically polymerized with benzoyl peroxide (~0.19 gr) as an initiator at around 65°C for 2 hours to produce microencapsulated granules²⁵. To reduce and increase the homogeneity of grain size, the mixture was ultrasonicated (22 kHz and 150 W)²³. Subsequently, filtration and washing with dilute water were performed to separate the granules from the solution. These granules were tested for characterization and then used for the adsorption experiment to study the competitive adsorption of lanthanum (La³⁺), cerium (Ce³⁺), and neodymium (Nd³⁺).

2.3. Characterization

Microencapsulation characterization was measured by calculating the encapsulation yield (yield%). The encapsulation yield was calculated by comparing the weight of the microencapsulation formed with the weight of the initial raw material (Equation 1)²².

$$yield (\%) = \frac{W_2}{W_1} \times 100 \quad (1)$$

The swelling test was conducted at room temperature for 24 hours. Approximately 0.5-2 grams of beads were immersed in 15 mL of deionized water until allowed to swell. Furthermore, the beads were vacuumed and filtered for about 1 hour until all the water was removed and weighed to obtain the wet beads. The wet beads were then allowed to dry at room temperature and dried in a vacuum oven at 45 °C for 2 days. After drying, the beads were reweighed to obtain the dry weight. Calculating the swelling ratio (%) follows Equation 2²⁹.

$$ratio\ swelling (\%) = \frac{w_{wet} - w_{dry}}{w_{dry}} \times 100\% \quad (2)$$

As KBr pellets, the dried samples' Fourier transform infrared (FTIR) spectra were measured by FTIR spectrophotometer (type Bruker Sensor 27) to analyze the surface functional groups present in poly(methyl methacrylate)-co-diacrylate/SWCNT nanocomposite and to evaluate the emulsion polymerization that occurs between octadecyl amine functionalized single-walled carbon nanotubes (ODA-SWCNT) and reactive mesogen diacrylate (RM257) with methyl methacrylate (MMA) before and after adsorption. The effective identification of carbon nanotubes (CNTs) in samples was achieved using the Raman spectroscopy test from HORIBA, the LabRAM HR Evolution Raman Microscope. The surface morphology was examined using the scanning electron microscope (SEM), and elemental mapping analysis was achieved by the scanning electron microscope-energy-dispersive X-ray spectrometer (SEM-EDS) from Jeol,

JSM-6510LA. Using a Quantachrome Nova 4200e analyzer, the Brunauer-Emmett-Teller (BET) method was used to determine the surface area of the adsorbent pores.

2.4. Adsorption Experiments

The adsorption experiment using the batch method was carried out at room temperature (25 °C), as shown in Figure 2. Adsorbent sample (100 mg) was immersed in the initial concentration of the rare earth elements (REEs) mixture in 20 mL of a multi-element solution of 0.5 mg/L and varying contact times (30, 60, 90, and 120 minutes) at pH 3.0 to examine the competitive kinetics of adsorption. At pH 5, the adsorption isotherm was measured, and the initial concentration of the REEs was between 0.5 and 6 mg/L. After the adsorption, ultraviolet-visible spectroscopy (UV-VIS) at wavelength 250 – 350 nm³⁰ as competitive adsorption reinforcing data, which was only carried out at pH 3, and inductively coupled plasma optical emission spectrometry (ICP-OES). The remaining lanthanum (La³⁺), cerium (Ce³⁺), and neodymium (Nd³⁺) concentrations were determined. The adsorption capacity of REE ion adsorbed (qt) and adsorption efficiency (η%) were calculated using Equations (3) and (4), respectively^{31,32}.

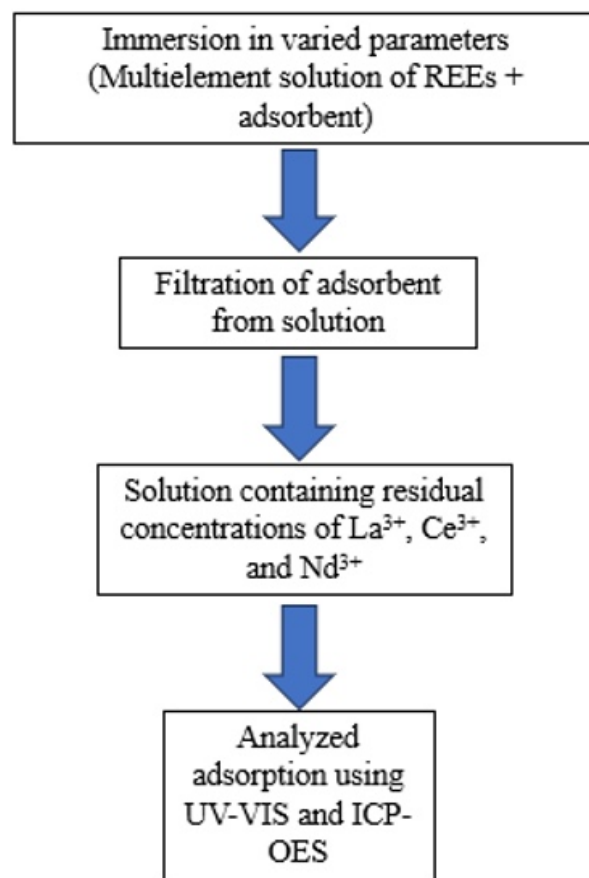


Fig. 2: Adsorption process of lanthanum (La³⁺), cerium (Ce³⁺), and neodymium (Nd³⁺) ions using poly(methyl methacrylate)-co-diacrylate/SWCNT nanocomposite adsorbent

$$q_t = \frac{V(c_0 - c_e)}{M} \quad (3)$$

$$\eta = \frac{c_0 - c_e}{c_0} \quad (4)$$

2.5. Kinetic and Isothermal Models of Adsorption

Kinetics was analyzed using Equations (5) and (6), the models' pseudo-first-order and pseudo-second-order nonlinear forms, respectively^{32,33}.

$$\ln(q_e - q_t) = \ln q_e - k_1 t \quad (5)$$

$$\frac{t}{q_t} = \frac{1}{k_2 q_e^2} + \frac{t}{q_e} \quad (6)$$

The Langmuir (Equation (7)) and Freundlich isotherm models (Equation (8)) were used to study the adsorption isotherm^{32,33}.

$$\frac{1}{q_e} = \frac{1}{q_m} + \left(\frac{1}{K_L q_m}\right) \left(\frac{1}{c_e}\right) \quad (7)$$

$$\ln q_e = \ln K_f + \frac{1}{n} \ln C_e \quad (8)$$

The adsorption processes, such as chemical adsorption ($n < 1$), linear adsorption ($n = 1$), or physical adsorption ($n > 1$), can be predicted using the adsorption intensity (n) Freundlich model³³.

3. Results and discussion

3.1. Characterization

The encapsulation yield of the poly(methyl methacrylate)-co-diacrylate/SWCNT nanocomposite adsorbent is used to evaluate the effectiveness and efficiency of the encapsulation process. It also predicts reproducibility and regeneration potential. The results of this experiment obtained an average yield value of 12.00% ± 0.577%. These results indicate that the level of reproducibility was quite good because the low standard deviation indicates that the repetition of the microencapsulation process is relatively consistent for the microencapsulation process to be controlled and reproducible³⁴. However, this low value indicates that only part of the active material, i.e., octadecyl amine functionalized single-walled carbon nanotubes (ODA-SWCNT), is encapsulated in the secondary material (poly(methyl methacrylate)-co-diacrylate). These results indicate that the adsorbent contains components consisting of ODA-SWCNT as the active material and poly(methyl methacrylate)-co-diacrylate as the secondary material. The Fourier transform infrared (FTIR) and Raman characterization results confirm these components' existence.

The swelling test on the adsorbent obtained the swelling degree at 0.133%. This means that the stability of

poly(methyl methacrylate)-co-diacrylate/SWCNTs nanocomposite adsorbent material is high because it is not easily brittle, does not experience significant changes, and its pore structure is maintained. With the high mechanical stability of the material, the adsorbent has high reproducibility and regeneration potential. It is possible to use it several times or for multiple adsorption-desorption cycles.

Fourier transform infrared (FTIR) spectra before adsorption (Figure 4: top part) results of the frequency peaks of the poly(methyl methacrylate)-co-diacrylate/SWCNT nanocomposite adsorbent were at 3449, 3001–2952, 1734, 1654, 1440, 1162–1069, and 992–647 cm⁻¹, each of which was the O-H, C-H, C=O, C=C, C-H, C-O, C=C, and C-H³⁵⁻³⁸. The C-H group indicates an alkane group from PMMA at 3001–2952 cm⁻¹^{35,37}. In other literature, these peaks indicate carbon nanotubes/polymethyl methacrylate (CNTs/PMMA) composites³⁸. C-H groups were also present at 1440, 992, 844, and 751 cm⁻¹ of PMMA-CNT³⁸. The peak of 1721 cm⁻¹ contained C=O, indicating the presence of carbonyl groups from PMMA³⁵, PMMA-CNT³⁸, and reactive mesogen diacrylate (RM 257)³⁶. C-O groups were also present at peaks 1162 and 1069 cm⁻¹, indicating the presence of acrylic groups from PMMA³⁵. The peak of 3449 cm⁻¹ contained the O-H group, indicating the presence of the vinyl groups from polyvinyl pyrrolidone (PVP)³⁷. Benzoyl peroxide (BPO) is generally indicated at a peak of 2960 cm⁻¹³⁷. However, this peak is not visible. The lack of indication of BPO proves that the BPO on the surface of the adsorbent has dissolved into the water and does not stick to the surface of the adsorbent because, when making the emulsion, filtering is carried out to separate the water phase and the oil phase³⁷. From several indications, these peaks prove that mixing and emulsion polymerization occurred in the adsorbent of poly(methyl methacrylate)-co-diacrylate/SWCNT nanocomposite, as summarized in Table 1.

In addition, to prove that the mixture contains carbon nanotubes (CNTs), a Raman identification test was carried out. Raman spectra for the type of SWCNTs usually display two double resonance peaks, namely the D band (D-Band) at approximately 1350 cm⁻¹ and the G band (G-Band), which consists of two primary components, one peaking at around 1590 cm⁻¹ (G+) and another at approximately 1570 cm⁻¹ (G-)³⁹. In other literature, the double resonance peak Raman spectra for SWCNTs samples using a wavelength of 785 nm display the D band at ~1320–1370 cm⁻¹ and the G band at ~1580 cm⁻¹⁴⁰. The Raman results for the poly(methyl methacrylate)-co-diacrylate/SWCNTs nanocomposite in Figure 3 showed the highest peak in the D band at 1345.61 cm⁻¹ and the G band at 1580.81 cm⁻¹. Thus, these peaks prove that CNTs are contained in the adsorbent.

In Fourier transform infrared (FTIR) after adsorption

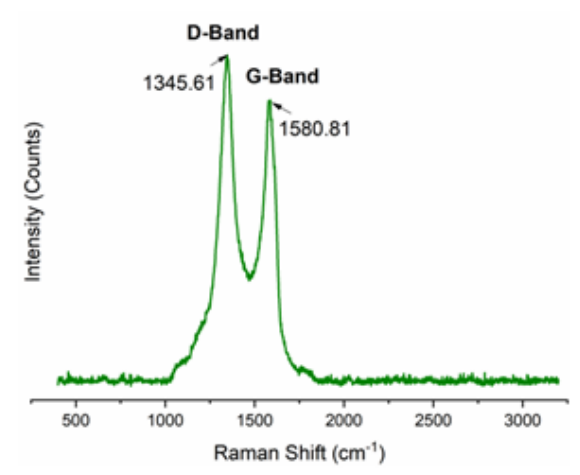


Fig. 3: Raman spectra of poly(methyl methacrylate)-co-diacrylate/SWCNTs nanocomposite adsorbent

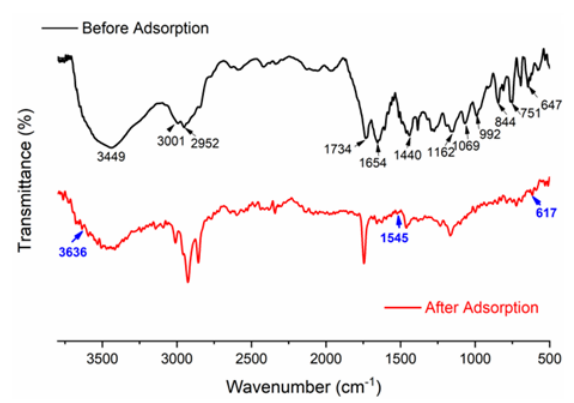


Fig. 4: Fourier transforms infrared (FTIR) spectra before and after adsorption of poly(methyl methacrylate)-co-diacrylate/SWCNTs nanocomposite adsorbent

(Figure 4), new peaks were visible at 3636, 1545, and 617 cm^{-1} . These summits' distinguishing peaks confirmed that La^{3+} , Ce^{3+} , and Nd^{3+} were successfully adsorbed into the poly(methyl methacrylate)-co-diacrylate/SWCNTs nanocomposite framework structure^{31,41,42}. The peaks resulting from metal ion adsorbates are not significantly visible. Still, the effect of interaction with the adsorbent is visible in the carbonyl group at 1734 cm^{-1} and the benzene group at 2928 and 2858 cm^{-1} . This result is strengthened by morphological analysis (Figure 6) and mapping by scanning electron microscope-energy-dispersive X-ray spectrometer (SEM-EDS) (Figs. 7 and 8), and is also supported by the FTIR spectrum identification listed in Table 1.

The morphology of poly(methyl methacrylate)-co-diacrylate/SWCNT nanocomposite structures before and after adsorption is shown in Figure 5. The structure of the poly(methyl methacrylate)-co-diacrylate/SWCNT nanocomposite adsorbent changed significantly after adsorption. After adsorption on this adsorbent's surface, a clear porous texture appeared with various pore sizes. This proves that the rare earth element (REE) molecules

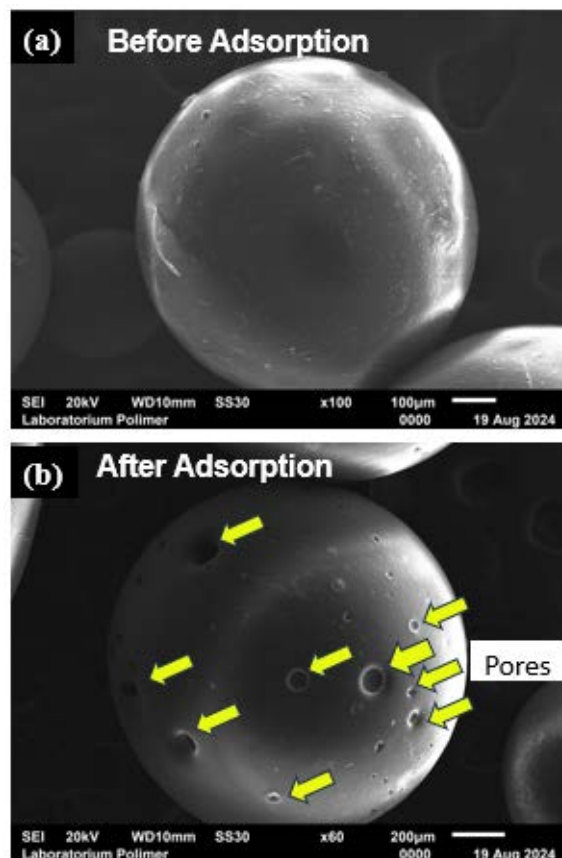


Fig. 5: Scanning electron microscope (SEM) image of poly(methyl methacrylate)-co-diacrylate/SWCNTs nanocomposite adsorbent. (a). Before adsorption (b). After adsorption

Table 1: Fourier transform infrared (FTIR) spectrum identification for poly (methyl methacrylate)-co-diacrylate/SWCNTs nanocomposite adsorbent

Peak frequency (cm^{-1})		Functional groups
Before adsorption	After adsorption	
-	3636	REE-O
3449	3449	O-H
3001	3011	C-H
2952	2928; 2858	C-H (vibration of CH in aromatic)
1734	1746	C=O (carbonyl)
1654	1658	C=C
-	1545	REE-O
1440	1462	C-H
1162	1167	C-O (acrylic group)
1069	1061	C-O (acrylic group)
992; 844. 752; 647	999; 827 752	C-H
-	617	REE-O

(adsorbates) have occupied the adsorbent's surface's active sites or pores, sticking to or interacting with the surface. Apart from that, the scanning electron microscope (SEM) morphology results indicated that the particle size of the adsorbent after adsorption was larger than before

Table 2: The particle size of poly (methyl methacrylate)-co-diacrylate/SWCNTs nanocomposite adsorbent

Adsorbent type	Average of area (μm ²)	Average length (μm)
Before adsorption	1.178	806.3
After adsorption	2.067	1.450

Table 3: Brunauer-Emmett-Teller (BET) results on poly(methyl methacrylate)-co-diacrylate/SWCNTs nanocomposite adsorbent

Adsorbent type	Pore radius (Å)	Pore volume (x 10 ⁻² cc/g)	Surface area (m ² /g)
Before adsorption	14.48	1.044	4.784
After adsorption	14.48	2.253	10.34

adsorption (Table 2). The following Brunauer-Emmett-Teller (BET) results reinforce this. Brunauer-Emmett-Teller (BET) characterization in Table 3 results on the pore surface upon adsorption of the adsorbent showed that the adsorbent's surface area and pore volume increased, but the pore radius did not change. This allows several indications, including the adsorbate molecules layering the adsorbent's surface by forming multilayers or expanding because of the adsorbate molecules inside the adsorbent diffusing into the adsorbent pores.

Figures 6 and 7 displayed the scanning electron microscope-energy-dispersive X-ray spectrometer (SEM-EDS) elemental mappings of poly(methyl methacrylate)-co-diacrylate/SWCNT nanocomposite before and after adsorption samples.

The before-adsorption EDS spectrum and the scanning electron microscope-energy-dispersive X-ray spectrometer (SEM-EDS) elemental mapping pictures are shown in Figure 7, indicating that these compositional elements of carbon (C) and oxygen (O) are uniformly distributed. A few apparent alterations in the after-adsorption sample were seen in Figure 8. In this case, there was an additional blue colour as an elemental mapping of lanthanum (La³⁺), cerium (Ce³⁺), and neodymium (Nd³⁺) ions whose intensity was lower than the intensity of carbon (C) and oxygen (O) ions indicated by small blue dots evenly distributed on the sample surface. The low intensity of REEs distributed in the form of small spots is likely a component with a low concentration that is adsorbed and distributed quite homogeneously on the surface of the adsorbent. The well-distributed La³⁺, Ce³⁺, and Nd³⁺ on the poly(methyl methacrylate)-co-diacrylate/SWCNTs nanocomposite after-adsorption surface indicate that the

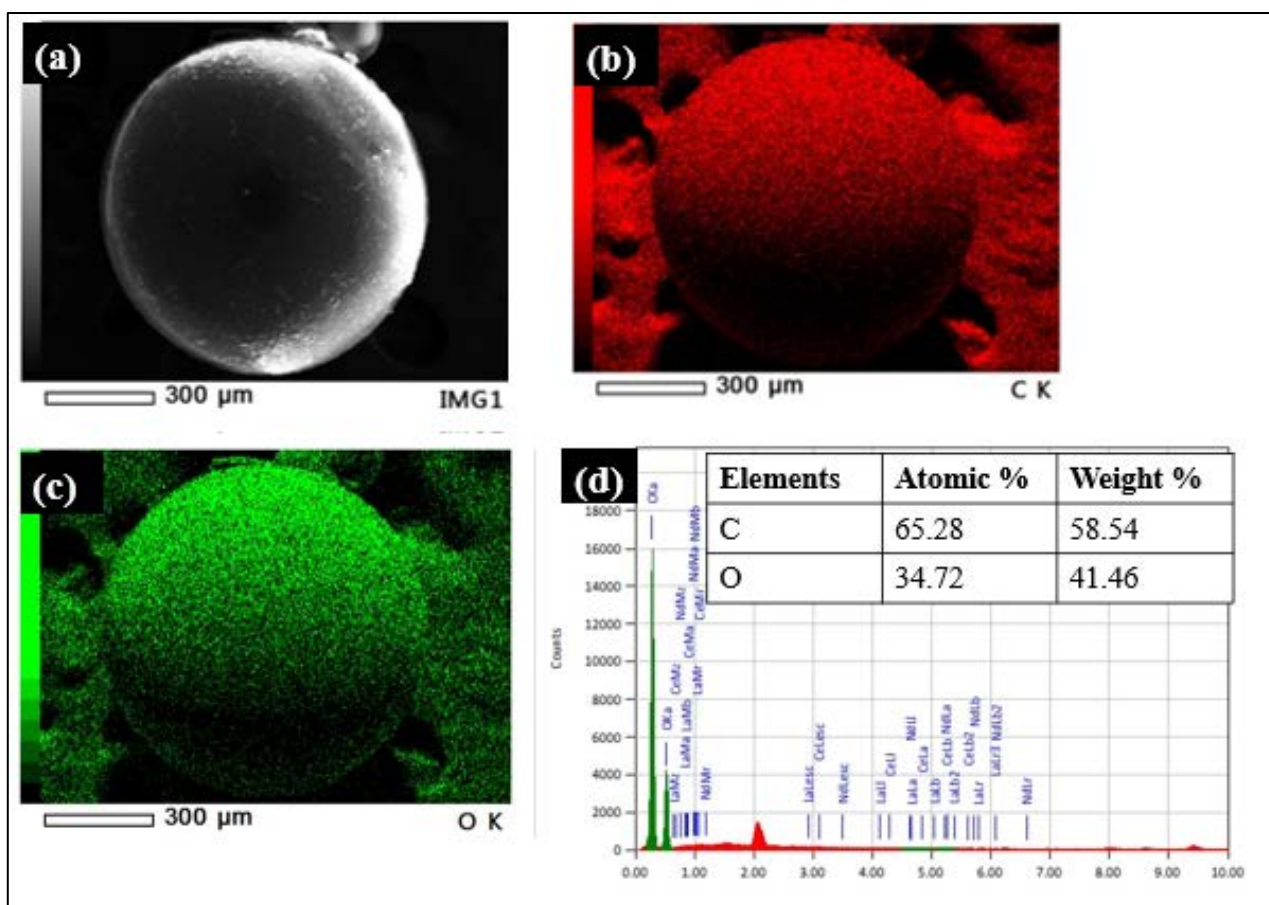


Fig. 6: Elemental mapping analysis of poly(methyl methacrylate)-co-diacrylate/SWCNTs nanocomposite adsorbent using scanning electron microscope-energy-dispersive X-ray spectrometer (SEM-EDS) before adsorption. (a). Secondary electron image of the adsorbent sample, (b). Carbon (C), (c). Oxygen (O) elements, (d). Area EDS spectrum and table of atomic and weight percentage of elements

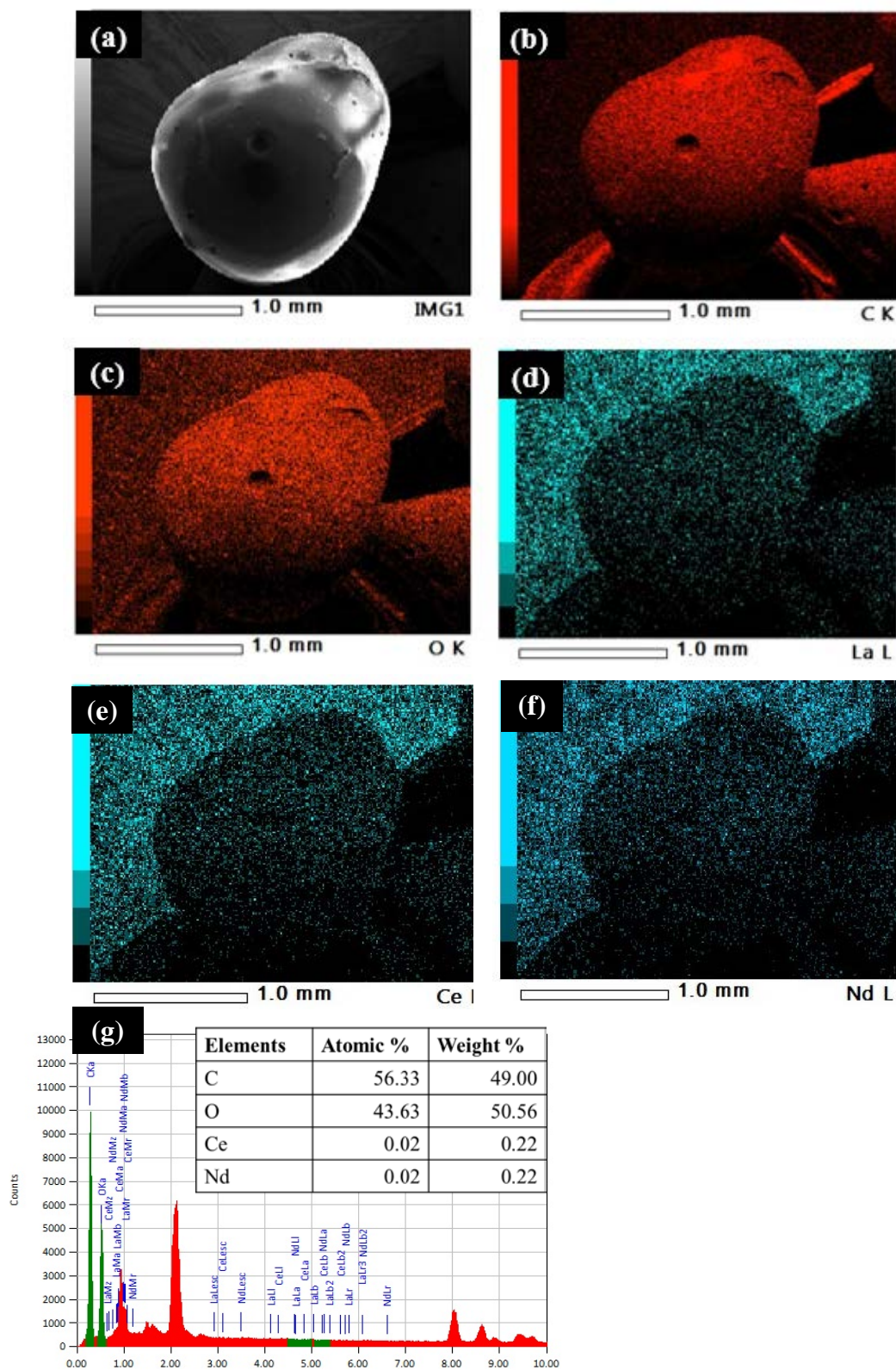


Fig. 7: Elemental mapping analysis of poly(methyl methacrylate)-co-diacrylate/SWCNTs nanocomposite adsorbent using scanning electron microscope-energy-dispersive X-ray spectrometer (SEM-EDS) after adsorption. (a). Secondary electron image of adsorbent sample; (b). Carbon (C); (c). Oxygen (O); (d). Lanthanum (La); (e). Cerium (Ce); (f). Neodymium (Nd) elements; (g). Area EDS spectrum and table of atomic and weight percentage of different elements

metal ions were successfully adsorbed on the adsorbent. This is also evidenced by the percentage values of atoms and masses of Ce^{3+} and Nd^{3+} elements, which are 0.02%

and 0.22%, respectively. On the other hand, only ion La^{3+} was not detected. This is likely due to several factors, including the spectrum which overlaps with the Ce^{3+} X-ray

peak, which has almost the same energy but is higher than La³⁺ (Ce³⁺ at 4,839 keV > La³⁺ at 4,650 keV) and the presence of more La³⁺ in the pores of the adsorbent than the adsorbent's surface. The results of the next section's kinetic and isothermal adsorption mechanism can strengthen this analysis.

3.2. Kinetics of adsorption and isotherm

Based on ultraviolet-visible spectroscopy (UV-VIS) measurements with a wavelength range of 250-350 nm, the optimal UV-VIS standard absorption was obtained at a wavelength of 250 nm with the lowest concentration that could be detected at a concentration of 4 ppm of the rare earth element (REE) standard mix solution. Furthermore, UV-VIS observations with a wavelength of 250 nm were carried out on the REEs feed solution after adsorption with a contact time of 30-120 minutes. The observations showed that UV-VIS absorbances could be measured on samples with a maximum contact time of 30 minutes. Contact times of more than 30 minutes were not detected. This indicates that the adsorbate has been significantly adsorbed after the first 30 minutes. To determine the adsorption efficiency quantitatively, measurements were then carried out using inductively coupled plasma optical emission spectrometry (ICP-OES).

Adsorption efficiency of lanthanum (La³⁺), cerium (Ce³⁺), and neodymium (Nd³⁺) versus the initial pH (3-6) from the results of the inductively coupled plasma optical emission spectrometry (ICP-OES) was shown in Figure 8.

Figure 8 showed that at pH 3, there was a significant difference in the percentage of adsorption efficiency of lanthanum (La³⁺), cerium (Ce³⁺), and neodymium (Nd³⁺) with values of 41.99%, 24.90%, and 33.11%, respectively. Therefore, in this study, we used pH 3 to determine the competitive adsorption of La³⁺, Ce³⁺, and Nd³⁺, as seen from the adsorption rate in the kinetic adsorption models. The optimum pH (pH 5) was used to determine the interaction between the adsorbent and adsorbate (chemical

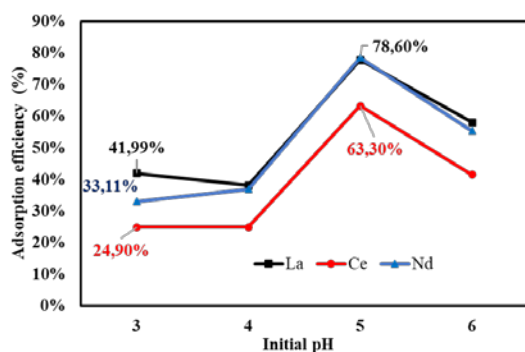


Fig. 8: Effect of acidity degree (pH) on adsorption efficiency of lanthanum (La³⁺), cerium (Ce³⁺), and neodymium (Nd³⁺) ions using the poly(methyl methacrylate)-co-diacrylate/SWCNT nanocomposite adsorbents

or physical adsorption) and the maximum adsorption capacity obtained under isotherm adsorption conditions. By comparing the coefficient correlation value (R²) between the pseudo-first-order and pseudo-second-order kinetic models, the fitting kinetics of adsorption models of rare earth elements (REEs) may be determined, and the poly(methyl methacrylate)-co-diacrylate/SWCNT nanocomposite adsorbents were identified. Linear regression plot results with an R² value closer to 1.00 as a suitable kinetic model for REE adsorption on poly(methyl methacrylate)-co-diacrylate/SWCNT nanocomposite adsorbents. The pseudo-first- and pseudo-second-order models were used to study the two-step adsorption kinetic process.

Figure 9 was the result of fitting the pseudo-first-order adsorption kinetic model of the poly(methyl methacrylate)-co-diacrylate/SWCNT nanocomposite adsorbents with these kinetic parameters in Table 4. Meanwhile, Figure 10 was the result of fitting the pseudo-second-order adsorption kinetic model of the poly(methyl methacrylate)-co-diacrylate/SWCNT nanocomposite adsorbents with these kinetic parameters in Table 5. According to the pseudo-first-order, the adsorbate has been moved to the surface of the adsorbent from the bulk solution containing rare earth elements (REEs). Pseudo-

Table 4: Adsorption kinetics parameters of pseudo-first-order models for lanthanum (La³⁺), cerium (Ce³⁺), and neodymium (Nd³⁺) ions utilizing poly(methyl methacrylate)-co-diacrylate/SWCNTs nanocomposite adsorbent

Ions	Parameters	
	k ₁ (min ⁻¹)	R ²
La ³⁺	0.0010 x 10 ⁻⁴	0.9085
Ce ³⁺	3.7150 x 10 ⁻⁴	0.8712
Nd ³⁺	6.6217 x 10 ⁻⁴	0.8936

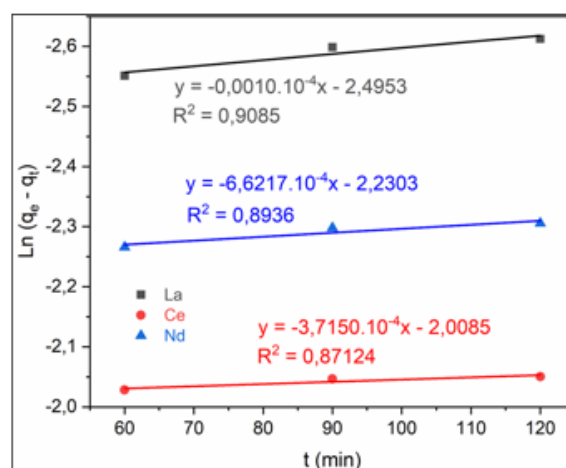


Fig. 9: Fitting of pseudo-first-order adsorption kinetic model of lanthanum (La³⁺), cerium (Ce³⁺), and neodymium (Nd³⁺) ions using the poly(methyl methacrylate)-co-diacrylate/SWCNT nanocomposite adsorbents

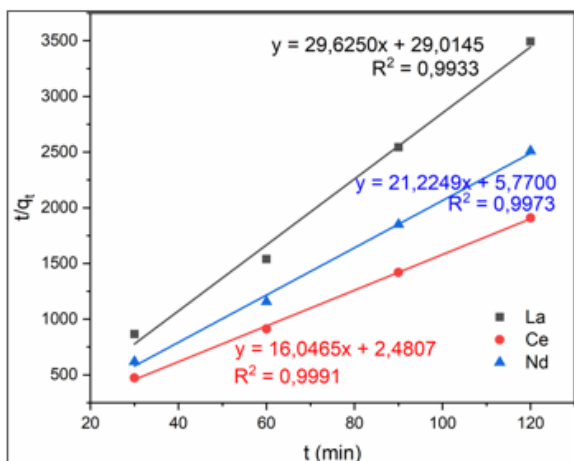


Fig. 10: Fitting of pseudo-second-order adsorption kinetic model of lanthanum (La³⁺), cerium (Ce³⁺), and neodymium (Nd³⁺) ions using the poly(methyl methacrylate)-co-diacrylate/SWCNT nanocomposite adsorbents

Table 5: Adsorption kinetics parameters of pseudo-second-order models for lanthanum (La³⁺), cerium (Ce³⁺), and neodymium (Nd³⁺) ions utilizing poly(methyl methacrylate)-co-diacrylate/SWCNTs nanocomposite adsorbent

Ions	Parameters	
	k ₂ (g/mg·min ⁻¹)	R ²
La ³⁺	29.625	0.9933
Ce ³⁺	16.047	0.9991
Nd ³⁺	21.225	0.9973

second-order presumes that the adsorbate was diffused and arranged inside the sorbent pores³³). In the first stage, these third elements from the solution have been transferred and attached to the adsorbent's surface. Then, in the second stage, metal ions were dissolved and arranged into the pores of the sorbent. The second stage was more successful than the first stage. This was proven by the value of the linear correlation coefficient (R²) of lanthanum (La³⁺), cerium (Ce³⁺), and neodymium (Nd³⁺), which had the values of pseudo-first-order, 0.9085, 0.8712, and 0.8936, respectively, lower than the value of pseudo-second-order, 0.9933, 0.9991, and 0.9973. Therefore, we find that the adsorption of REEs on poly(methyl methacrylate)-co-diacrylate/SWCNTs nanocomposite adsorbents followed pseudo-second-order.

From the results of this adsorption kinetics modelling, we also found that there was competitive adsorption of the three rare earth elements (REEs), lanthanum (La³⁺), cerium (Ce³⁺), and neodymium (Nd³⁺). The values of the kinetic rate of the first stage (pseudo-first-order) for La³⁺, Ce³⁺, and Nd³⁺ were 0.0010 x 10⁻⁴, 3.7150 x 10⁻⁴, and 6.6217 x 10⁻⁴ min⁻¹, respectively. We found that the order of the adsorption rate from the bulk solution to the sorbent surface ranges from the highest to the lowest, i.e., Nd³⁺, Ce³⁺, and La³⁺ ions, respectively. In this case, the value of La³⁺ is significantly lower than that of Ce³⁺ and Nd³⁺.

Meanwhile, the kinetic rate values of the second stage (pseudo-second-order) for La³⁺, Ce³⁺, and Nd³⁺ were 29.625, 16.047, and 21.225 g/mg·min⁻¹, respectively. We found that the order of the adsorption diffusion rate in the sorbent pores ranges from highest to lowest for La³⁺, Nd³⁺, and Ce³⁺ ions, respectively. In this case, the adsorption rate of La³⁺ in the first stage (pseudo-first-order) was the lowest of Ce³⁺ and Nd³⁺. Meanwhile, the adsorption rate of La³⁺ in the second stage (pseudo-second order) was the highest of Ce³⁺ and Nd³⁺. These results indicate that La³⁺ moves very slowly into the adsorbent surface. However, La³⁺ ions diffuse through the adsorbent pores more quickly during the second stage than other ions. Therefore, the presence of La³⁺ ions is less than Ce³⁺ and Nd³⁺ ions on the adsorbent surface, and the presence of La³⁺ ions is mainly in the pores of the adsorbent, possibly undetected La³⁺ ions on the adsorbent's surface. This analysis is also reinforced by the results of SEM-EDS mapping in the previous discussion.

The significance of adsorption isotherms in explaining how the solute interacts with the adsorbent and the transfer of adsorbate from the phases of liquid to solid upon reaching the equilibrium state of the adsorption process, whether a monolayer or multilayer is formed^{33,43}). Isotherm models, including Langmuir and Freundlich, were studied for this analysis. The first model (Langmuir) applies to monolayer adsorption onto surfaces with a limited number of similar adsorbent sites, whereas the second model (Freundlich) applies to multilayer adsorption on heterogeneous surfaces^{33,43}).

Figure 11 was the result of fitting the Langmuir adsorption isotherm model of the poly(methyl methacrylate)-co-diacrylate/SWCNT nanocomposite adsorbents with these isotherm parameters in Table 6. Meanwhile, Figure 12 was

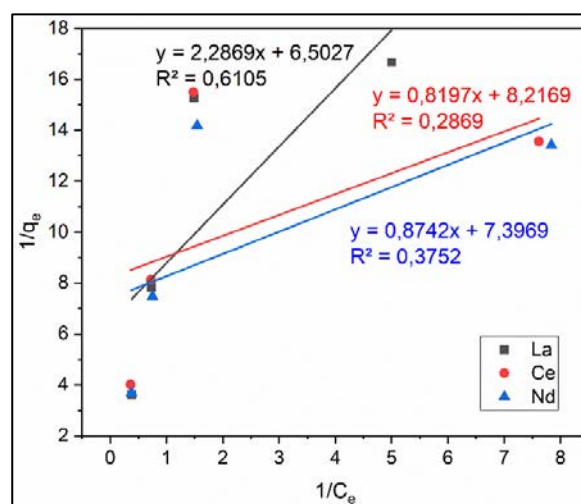


Fig. 11: Fitting of Langmuir adsorption isotherm model of lanthanum (La³⁺), cerium (Ce³⁺), and neodymium (Nd³⁺) ions using the poly(methyl methacrylate)-co-diacrylate/SWCNT nanocomposite adsorbents

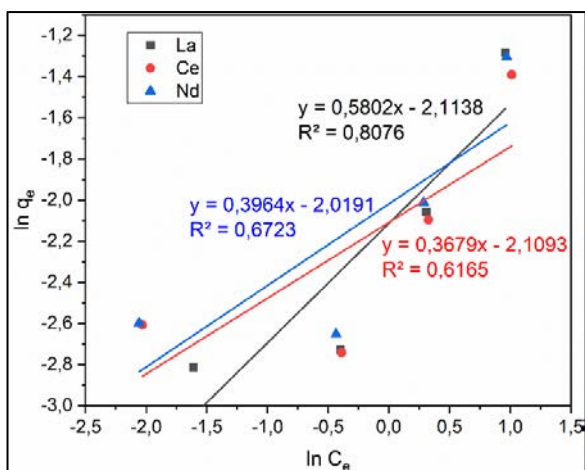


Fig. 12: Fitting of Freundlich adsorption isotherm model of lanthanum (La³⁺), cerium (Ce³⁺), and neodymium (Nd³⁺) ions using the poly(methyl methacrylate)-co-diacrylate/SWCNT nanocomposite adsorbents

Table 6: Adsorption isotherm parameters of the Langmuir model for lanthanum (La³⁺), cerium (Ce³⁺), and neodymium (Nd³⁺) ions utilizing poly(methyl methacrylate)-co-diacrylate/SWCNTs nanocomposite adsorbent

Ions	Parameters		
	K _L	R ²	q _m (mg/g)
La ³⁺	2.8434	0.6105	0.1538
Ce ³⁺	10.024	0.2869	0.1217
Nd ³⁺	8.4613	0.3752	0.1352

Table 7: Adsorption isotherm parameters of the Freundlich model for lanthanum (La³⁺), cerium (Ce³⁺), and neodymium (Nd³⁺) ions utilizing poly(methyl methacrylate)-co-diacrylate/SWCNTs nanocomposite adsorbent

Ions	Parameters		
	K _F	R ²	n
La ³⁺	0.1208	0.8076	1.7235
Ce ³⁺	0.1213	0.6165	2.7181
Nd ³⁺	0.1328	0.6723	2.5227

the result of fitting the Freundlich adsorption isotherm model of the poly(methyl methacrylate)-co-diacrylate/SWCNT nanocomposite adsorbents with these kinetic parameters in Table 7. After comparing the correlation coefficient values (R²) of adsorption isotherm models, the adsorption process of lanthanum (La³⁺), cerium (Ce³⁺), and neodymium (Nd³⁺) follows the Freundlich model. This means that the interaction between the adsorbate and the adsorbent is physical adsorption, and the type of layer formed tends to be multilayer. This is proven by the value of n > 1 for La³⁺, Ce³⁺, and Nd³⁺. The Langmuir isotherm results show that lanthanum (La³⁺) had the highest maximum adsorption capacity compared to other ions, followed by neodymium (Nd³⁺) and cerium (Ce³⁺), i.e., 0.15381, 0.1352, and 0.1217 mg/g, respectively. These results are consistent with adsorption kinetics results and are reinforced by the SEM-EDS results in the previous section.

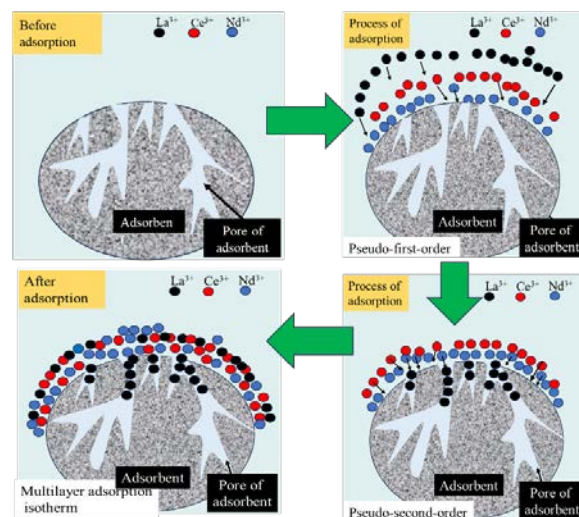


Fig. 13: A schematic representation of the adsorption mechanism of the poly(methyl methacrylate)-co-diacrylate/SWCNT nanocomposite adsorbent

Table 8: A comparison of the adsorption characterization of p(HEMA-CNT/CNC) and poly(methyl methacrylate)-co-diacrylate/SWCNT

Parameters	Nanocomposite adsorbent		
	P(HEMA-CNT/CNC) ¹⁴⁾	Poly (methyl methacrylate)-co-diacrylate/SWCNT	
Content of CNTs-	0.5 wt.%	0.05 wt.%	
Functional group	Higher O-H	Low O-H	
Pore radius (Å)	70.28	14.48	
Pore volume (x 10 ⁻² cc/g)	4.871	1.044	
Surface area (m ² /g)	19.09	4.784	
Form of adsorbent (Figure 14)	Thin membrane	Granular or bead	
Kinetic rates	Pseudo first order - k ₁ (min ⁻¹)		
	La ³⁺	0.0050	0.0010 x 10 ⁻⁴
	Ce ³⁺	0.0016	3.7150 x 10 ⁻⁴
	Nd ³⁺	0.0018	6.6217 x 10 ⁻⁴
	Pseudo second order - k ₂ (g/mg·min ⁻¹)		
	La ³⁺	0.1194	29.625
	Ce ³⁺	1.2728	16.047
Nd ³⁺	1.1669	21.225	
Adsorption capacities (mg/g)	La ³⁺	0.6488	0.1538
	Ce ³⁺	0.8927	0.1217
	Nd ³⁺	0.8545	0.1352
Layer formed	monolayer	multilayer	

Figure 13 shows a schematic representation of the poly(methyl methacrylate)-co-diacrylate/SWCNT nanocomposite adsorbent's adsorption mechanism. In addition, we have conducted research on other nanocomposite adsorbents, namely p(HEMA-CNT/CNC), fabricated of SWCNT, 2-hydroxyethyl methacrylate (HEMA), and cellulose nanocrystals (CNC). Both use the

same adsorption mechanism analysis method, i.e., the fitting of adsorption kinetic models (pseudo-first and second order) and adsorption isotherm models (Langmuir and Freundlich) on the adsorption of rare earth element (REE) ions, especially lanthanum (La³⁺), cerium (Ce³⁺) and neodymium (Nd³⁺). A comparison of the two nanocomposite adsorbents, poly(methyl methacrylate)-co-diacrylate/SWCNT and p(HEMA-CNT/CNC), can be seen in Table 8.

Based on Table 8, the adsorption capacity of the p(HEMA-CNT/CNC) nanocomposite adsorbent was superior to poly(methyl methacrylate)-co-diacrylate/SWCNT. This is due to various factors, including the percentage of carbon nanotubes (CNTs) in poly(methyl methacrylate)-co-diacrylate/SWCNT being very small (0.05% wt.%), so it is unable to adsorb rare earth element (REE) ions optimally. The functional group of poly(methyl methacrylate)-co-diacrylate/SWCNT containing oxygen was very low, which makes it difficult for ion exchange or chemical adsorption between the adsorbent surface and REE ions. The surface area, size, and pore volume of the poly(methyl methacrylate)-co-diacrylate/SWCNT adsorbent were lower than the p(HEMA-CNT/CNC) adsorbent. The low surface area makes it more difficult for REE ions to adhere to its surface, so the amount adsorbed is lower^{11,44,45}. However, the mechanical stability of poly(methyl methacrylate)-co-diacrylate/SWCNT was superior to p(HEMA-CNT/CNC), as shown in Figure 14. The thin and fragile shape of p(HEMA-CNT/CNC) membrane requires a complex separation process because the adsorbent is dispersed in water media, which causes the filtration process uses a small pore size.

We also analyzed the environmental impact by comparing the traditional methods, such as liquid-liquid extraction (LLE) against the poly(methyl methacrylate)-co-diacrylate/SWCNT nanocomposite adsorbent using the nanocomposite-based adsorption method in solid phase extraction (SPE) in the extraction of rare earth metals (Table 9).

In this study, we also calculated the estimated cost of the poly(methyl methacrylate)-co-diacrylate/SWCNT

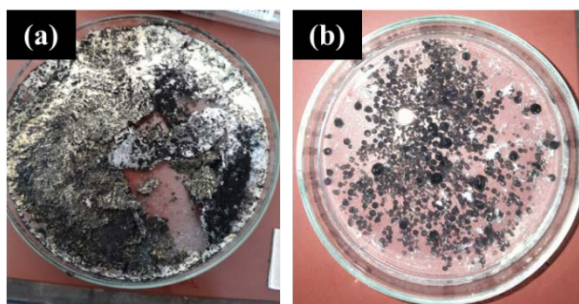


Fig. 14: Type of nanocomposite adsorbent form. (a). Poly(methyl methacrylate)-co-diacrylate/SWCNT, (b). P(HEMA-CNT/CNC)

Table 9: Environmental impact comparison of traditional liquid-liquid extraction (LLE) and innovative nanocomposite-based adsorption in solid-phase extraction (SPE) methods

Parameters	Traditional method	Innovative method
Consumption of organic solvent	High, using solvents such as H ₂ SO ₄ , HCl, NaOH, and/or HNO ₃ in large quantities to produce high extraction efficiency so that it is carried out repeatedly ⁴⁶ .	Very low, using methyl methacrylate (MMA) and nitric acid (HNO ₃) at low concentrations (3%), both in small amounts during elution carried out in one cycle/step.
Temperature of process	High, using high temperatures such as the leaching process of around 180–220 °C ⁴⁷ .	Low, using a temperature of around 65°C in the polymerization process and room temperature in the adsorption process.
Waste product	High, hazardous solvent waste ⁴⁶ .	Low, using a small amount of solvent waste.
Reproducibility and recycling potential	Low, solvents need complex purification.	Quite good, adsorbent can be reused.
Work safety	Low, using non-dangerous chemicals and processes at high temperatures.	High, using non-hazardous chemicals, and the process does not require high temperatures.

Table 10: The estimated unit cost of producing the poly(methyl methacrylate)-co-diacrylate/SWCNT nanocomposite adsorbent

Input	Value
Volumetric flowrate per day (mL)	180
Batch time (min)	60
Daily working hours (h/day)	3
Unit capacity calculation (mL)	36
Chemical consumption (USD/g)	34.264
Energy consumption (USD)	0.0965

nanocomposite adsorbent production process on a small scale of the laboratory, consisting of chemical consumption, energy consumption, and other cost (honorarium), to find out the feasibility and effectiveness of adsorbent production⁴⁸. The estimated cost of the poly(methyl methacrylate)-co-diacrylate/SWCNT nanocomposite adsorbent production process can be seen in Table 10.

From Table 10, the production capacity of poly(methyl methacrylate)-co-diacrylate/SWCNT nanocomposite

adsorbent was 54 Liters/year (3 batches x 60 mL x 300 working days). The estimated production cost of poly(methyl methacrylate)-co-diacrylate/SWCNT nanocomposite can be calculated by allocating 20% of the calculated cost for material and energy utilization as the overall cost⁴⁸). Based on this calculation, the poly(methyl methacrylate) production cost-co-diacrylate/SWCNT nanocomposite adsorbent is USD 793.16/m³. This cost is still higher than other nanocomposite adsorbents⁴⁸). The potential for reducing production costs so that they can be applied in the industry includes increasing production capacity by increasing batch volume, increasing adsorbent production efficiency (one of which is improving the encapsulation process method), implementing new, more efficient technology, and/or developing efficient regeneration methods for adsorbent reuse, and procuring raw materials in large quantities. Indonesia has a high potential for industrial-scale production due to using low-cost raw materials such as tin-related monazite minerals and electronic waste. This potential can decrease production costs.

4. Conclusions

A study on competitive lanthanum (La), cerium (Ce), and neodymium (Nd) ions on poly(methyl methacrylate)-co-diacrylate/SWCNT nanocomposite adsorbents has been conducted. The results of the experiment show that the surface of the poly(methyl methacrylate)/carbon nanotube nanocomposite adsorbents provide electrostatic interactions between rare earth element (REE) ions and functional groups that effectively adsorb REE³⁺ ions, such as C=O, with the interaction order from highest to lowest being La³⁺, Ce³⁺, and Nd³⁺. This is evident from a new oxide-rare earth elements (REEs-O) peak after adsorption at 3636, 1545, and 617 cm⁻¹ and the strengthening of the carbonyl and benzene group at 2928 and 2858 cm⁻¹ with the increasingly sharp peaks. In addition, the presence of increasingly clear pores and the detection of REE³⁺ ions from scanning electron microscope-energy-dispersive X-ray spectrometer (SEM-EDS) morphology and element mapping results. This is also supported by the results of ultraviolet-visible spectroscopy (UV-VIS) at a wavelength of 250 nm with contact time after 30 minutes and quantitatively by the results of inductively coupled plasma optical emission spectrometry (ICP-OES). In addition, we find that the competitive adsorption of La³⁺, Ce³⁺, and Nd³⁺ occurs at pH 3, which order based on the adsorption efficiency value is La³⁺ > Nd³⁺ > Ce³⁺, with the respective values of 41.99%, 33.11%, and 24.90%.

The results of the kinetic analysis show that poly(methyl methacrylate)/carbon nanotube nanocomposite adsorbents adhere to a pseudo-second-order kinetic model with order adsorption rates from highest to lowest being La³⁺ > Nd³⁺ > Ce³⁺ with values of 29.625, 21.225, and 16.047 min⁻¹,

respectively. This means that poly(methyl methacrylate)-co-diacrylate/SWCNT nanocomposite adsorbents provide easier diffusion and metal ions are arranged within the sorbent's pores rather than transferring and attaching to the surface of the adsorbent, where La³⁺ diffuses most quickly and efficiently into the pores, followed by Nd³⁺, and finally Ce³⁺.

The Freundlich model follows the process of adsorption, meaning that the interaction between rare earth element (REE) ions and poly(methyl methacrylate)-co-diacrylate/SWCNT nanocomposite adsorbents are physical adsorption, and a multilayer is formed on the surface of the adsorbent. The Langmuir model's highest order adsorption capacity is La³⁺ > Nd³⁺ > Ce³⁺ with values of 0.15381, 0.1352, and 0.1217 mg/g, respectively.

Based on the analysis results, poly(methyl methacrylate)-co-diacrylate/SWCNT nanocomposite adsorbents for recovery of rare earth element (REE) ions are currently suitable for low-concentration and small-scale application. However, their advantages in mechanical stability, ion selectivity at pH 3, and environmentally friendly, those adsorbents provide enormous potential for further development to make them fit industrial purposes, such as using the freeze-drying technique, optimization of the weight/dose ratio of adsorbents, and the concentration of REE ions in the feed solution.

Poly(methyl methacrylate)-co-diacrylate/SWCNT nanocomposite adsorbent has high commercialization potential, especially in Indonesia for the recovery of secondary waste such as tin-related monazite minerals and electronic waste, market needs for advanced components, and the need for environmentally friendly technology. In addition, this method has the potential to interact with other methods, such as at the final stage of the leaching method or secondary waste applications to adsorb rare earth element (REE) ion residues. Therefore, production cost optimization, extended research, and industry-research cooperation are required for large-scale implementation.

Acknowledgements

The authors acknowledge the facilities and scientific and technical support from the Research Center for Polymer Technology Laboratory, Nuclear Advanced Materials Laboratory, Advanced Physics Imaging Laboratory, and Advanced Characterization Laboratories Serpong National Research and Innovation Agency through E-Layanan Sains-BRIN. We thank Faculty of Mathematics and Natural Sciences Universitas Indonesia for funding this research through Hibah Riset FMIPA UI 2023-2024.

Nomenclature

C_e REEs concentration at equilibrium (mg/L) in the aqueous solution

C_0	concentration of REEs at the beginning of the experiment (mg/L)
k_1	first-order rate constants (min^{-1})
k_2	second-order rate constants ($\text{g/mg}\cdot\text{min}^{-1}$)
K_F	Freundlich isotherm constant
K_L	constant in Langmuir models
M	mass of the adsorbent (mg)
n	adsorption intensity
q_e	adsorption capacity at equilibrium (mg/g)
q_m	maximum adsorption capacity (mg/g)
q_t	adsorption capacity at any given time t (mg/g)
V	the total volume of the aqueous solution (mL)
W_1	the weight of the material used to produce the microencapsulation (mg)
W_2	the weight of the microencapsulation (mg)
W_{dry}	dry weight of beads (g)
W_{wet}	wet weight of beads (g)
$\eta\%$	Percentage of adsorption efficiency

References

- 1) E. Kusriani, M.I. Alhamid, D.A. Wulandari, M. Fatkhurrahman, E.W.E.S. Shahrin, N.N.M. Shahri, A. Usman, A.B. Prasetyo, M. Sufyan, A. Rahman, K.D. Nugrahaningtyas, and S.J. Santosa, "Simultaneous adsorption of multicomponent lanthanide ions on pectin encapsulated zeolite a," *Evergreen*, 11 (1) 371–378 (2024). doi:10.5109/7172296.
- 2) V. Balaram, "Rare earth elements: a review of applications, occurrence, exploration, analysis, recycling, and environmental impact," *Geosci. Front.*, 10 (4) 1285–1303 (2019). doi:10.1016/j.gsf.2018.12.005.
- 3) S.T. Huber, and K.W. Steininger, "Critical sustainability issues in the production of wind and solar electricity generation as well as storage facilities and possible solutions," *J. Clean. Prod.*, 339 (November 2021) 130720 (2022). doi:10.1016/j.jclepro.2022.130720.
- 4) I. Setiawan, "Towards the challenging ree exploration in indonesia," *IOP Conf. Ser. Earth Environ. Sci.*, 118 (1) (2018). doi:10.1088/1755-1315/118/1/012075.
- 5) A.Q. Mairizal, A.Y. Sembada, K.M. Tse, and M.A. Rhamdhani, "Electronic waste generation, economic values, distribution map, and possible recycling system in Indonesia," *J. Clean. Prod.*, 293 (2021). doi:10.1016/j.jclepro.2021.126096.
- 6) T. Liu, and J. Chen, "Extraction and separation of heavy rare earth elements: a review," *Sep. Purif. Technol.*, 276 (May) (2021). doi:10.1016/j.seppur.2021.119263.
- 7) A. Merroune, J. Ait Brahim, M. Berrada, M. Essakhraoui, B. Achoui, H. Mazouz, and R. Beniazza, "A comprehensive review on solvent extraction technologies of rare earth elements from different acidic media: current challenges and future perspectives," *J. Ind. Eng. Chem.*, 139 (January) 1–17 (2024). doi:10.1016/j.jiec.2024.04.042.
- 8) M. Asadollahzadeh, R. Torkaman, and M. Torab-Mostaedi, "Extraction and separation of rare earth elements by adsorption approaches: current status and future trends," *Sep. Purif. Rev.*, 00 (00) 1–28 (2020). doi:10.1080/15422119.2020.1792930.
- 9) C.E.D. Cardoso, J.C. Almeida, and T. Trindade, "Recovery of rare earth elements by carbon-based nanomaterials - a review recovery of rare earth elements by carbon-based nanomaterials — a review," (May) (2019). doi:10.3390/nano9060814.
- 10) Y. Hu, E. Drouin, D. Larivière, F. Kleitz, and F.G. Fontaine, "Highly efficient and selective recovery of rare earth elements using mesoporous silica functionalized by preorganized chelating ligands," *ACS Appl. Mater. Interfaces*, 9 (44) 38584–38593 (2017). doi:10.1021/acsami.7b12589.
- 11) N. Jamilah, A.B. Cahaya, and A. Riswoko, "Website : <http://ejournal.undip.ac.id/index.php/reaktor/> adsorption using selective adsorbents as an effective method for rare earth elements recovery – a review," 23 (3) 77–91 (2024).
- 12) X. Wei, J. Han, and W. Qin, "Research advances in low-concentration rare earth ion adsorption materials," *Gongcheng Kexue Xuebao/Chinese J. Eng.*, 46 (8) 1381–1392 (2024). doi:10.13374/j.issn2095-9389.2023.10.23.006.
- 13) C.E. Unsworth, C.C. Kuo, A. Kuzmin, S. Khalid, and D. Saha, "Adsorption of rare earth elements onto dna-functionalized mesoporous carbon," (2020).
- 14) N. Jamilah, A. Riswoko, and Adam Badra Cahaya, "Carbon nanotube modified poly hema/cnc composite sorbent for selective recovery of rare earth metal ions," *J. Sains Mater. Indones.*, 25 (2) 140–149 (2024). doi:10.55981/jsmi.2024.3134.
- 15) X. Wei, X. Mao, J. Han, W. Qin, and H. Zeng, "Novel nitrogen-rich hydrogel adsorbent for selective extraction of rare earth elements from wastewater," 479 (June) (2024).
- 16) A.S. Al-salem, A.A. Nayl, M.S. Alshammari, and I.M. Ahmed, "Adsorption study of neodymium from the aqueous phase using fabricated magnetic chitosan-functionalized graphene oxide composites," (2024). doi:10.1021/acsomega.4c04742.
- 17) M.E. Birch, T.A. Ruda-Eberenz, M. Chai, R. Andrews, and R.L. Hatfield, "Properties that influence the specific surface areas of carbon nanotubes and nanofibers," *Ann. Occup. Hyg.*, 57 (9) 1148–1166 (2013). doi:10.1093/annhyg/met042.
- 18) P.K. Sonkar, Narvdeshwar, and P.K. Gupta, "Characteristics of carbon nanotubes and their nanocomposites," *Fundam. Prop. Multifunct. Nanomater.*, (March) 99–118 (2021).

- doi:10.1016/B978-0-12-822352-9.00011-0.
- 19) C. Ménard-Moyon, K. Kostarelos, M. Prato, and A. Bianco, "Functionalized carbon nanotubes for probing and modulating molecular functions," *Chem. Biol.*, 17 (2) 107–115 (2010). doi:10.1016/j.chembiol.2010.01.009.
 - 20) M. Monthieux, B.W. Smith, B. Burteaux, A. Claye, J.E. Fischer, and D.E. Luzzi, "Sensitivity of single-wall carbon nanotubes to chemical processing: an electron microscopy investigation," *Carbon N. Y.*, 39 (8) 1251–1272 (2001). doi:10.1016/S0008-6223(00)00249-9.
 - 21) A. Nag, M.E.E. Alahi, S.C. Mukhopadhyay, and Z. Liu, "Multi-walled carbon nanotubes-based sensors for strain sensing applications," *Sensors (Switzerland)*, 21 (4) 1–22 (2021). doi:10.3390/s21041261.
 - 22) Fadilah, S. Distantina, A.D. Susanti, E. Fitriyani, and A.D. Damayanti, "Microencapsulation of rice bran oil by complex coacervation using chitosan – k-carrageenan: influence of glutaraldehyde and tween 20," *Evergreen*, 10 (1) 546–552 (2023). doi:10.5109/6782159.
 - 23) F. Ahangaran, A.H. Navarchian, and F. Picchioni, "Material encapsulation in poly(methyl methacrylate) shell: a review," *J. Appl. Polym. Sci.*, 136 (41) 1–21 (2019). doi:10.1002/app.48039.
 - 24) J.H.L. Voncken, "Physical and Chemical Properties of the Rare Earths," in: 2016: pp. 53–72. doi:10.1007/978-3-319-26809-5_3.
 - 25) R.A. Fraser, K. Stoeffler, B. Ashrafi, Y. Zhang, and B. Simard, "Large-scale production of pmma/swcnt composites based on swcnt modified with pmma," *ACS Appl. Mater. Interfaces*, 4 (4) 1990–1997 (2012). doi:10.1021/am201824k.
 - 26) M.G. Simões, P. Coimbra, A.S. Carreira, M.M. Figueiredo, M.H. Gil, and P.N. Simões, "Eugenol-loaded microspheres incorporated into textile substrates," *Cellulose*, 27 (7) 4109–4121 (2020). doi:10.1007/s10570-020-03010-2.
 - 27) M. Gericke, J. Trygg, and P. Fardim, "Functional cellulose beads: preparation, characterization, and applications," *Chem. Rev.*, 113 (7) 4812–4836 (2013). doi:10.1021/cr300242j.
 - 28) F. Ahangaran, M. Hayaty, A.H. Navarchian, and F. Picchioni, "Micromechanical assessment of pmma microcapsules containing epoxy and mercaptan as self-healing agents," *Polym. Test.*, 64 330–336 (2017). doi:10.1016/j.polymertesting.2017.10.014.
 - 29) N. Boudouaia, A.A. Bendaoudi, H. Mahmoudi, T. Saffaj, and Z. Bengharez, "Swelling and adsorption properties of crosslinked chitosan-based filmkinetic, thermodynamic and optimization studies," *Desalin. Water Treat.*, 255 (May 2021) 56–67 (2022). doi:10.5004/dwt.2022.28321.
 - 30) S.K. Sharma, T. Behm, T. Köhler, J. Beyer, R. Gloaguen, and J. Heitmann, "Library of uv-visible absorption spectra of rare except pm)," 4 (2020). doi:10.3390/cryst10070593.
 - 31) R.M. Ashour, H.N. Abdelhamid, A.F. Abdel-Magied, A.A. Abdel-Khalek, M.M. Ali, A. Uheida, M. Muhammed, X. Zou, and J. Dutta, "Rare earth ions adsorption onto graphene oxide nanosheets," *Solvent Extr. Ion Exch.*, 35 (2) 91–103 (2017). doi:10.1080/07366299.2017.1287509.
 - 32) L. Zhao, X. Duan, M.R. Azhar, H. Sun, X. Fang, and S. Wang, "Selective adsorption of rare earth ions from aqueous solution on metal-organic framework hkust-1," *Chem. Eng. J. Adv.*, 1 (June) (2020). doi:10.1016/j.cej.2020.100009.
 - 33) M.Alaqarbeh, "Adsorption phenomena: definition, mechanisms, and adsorption types: short review," *RHAZES Green Appl. Chem.*, 13 (September) 43–51 (2021). doi:10.48419/IMIST.PRSM/rhazes-v13.28283.
 - 34) N.V.N. Jyothi, P.M. Prasanna, S.N. Sakarkar, K.S. Prabha, P.S. Ramaiah, and G.Y. Srawan, "Microencapsulation techniques, factors influencing encapsulation efficiency," *J. Microencapsul.*, 27 (3) 187–197 (2010). doi:10.3109/02652040903131301.
 - 35) S.S. Suresh, S. Mohanty, and S.K. Nayak, "Investigation into the mechanical and thermal properties of poly(methyl methacrylate) recovered from light guidance panels with a focus on future remanufacturing and sustainable waste management," *J. Remanufacturing*, 7 (2–3) 217–233 (2017). doi:10.1007/s13243-017-0041-7.
 - 36) M.A. Kamarudin, A.A. Khan, C. Williams, G. Rughoobur, S.M. Said, S. Nosheen, A.J. Flewitt, M.M. Qasim, and T.D. Wilkinson, "Self-assembled liquid crystalline nanotemplates and their incorporation in dye-sensitised solar cells," *Electrochim. Acta*, 222 (December) 657–667 (2016). doi:10.1016/j.electacta.2016.11.021.
 - 37) M.A. Ariyanto, I. Zulfa, K.D. Hernugrahanto, Ferdiansyah, P.N. Trisanti, and Sumarno, "Purification process of poly methyl methacrylate products made with suspension polymerization techniques," *IOP Conf. Ser. Mater. Sci. Eng.*, 1053 (1) 012112 (2021). doi:10.1088/1757-899x/1053/1/012112.
 - 38) S.H.R. Ali, M.K. Bedewy, M.A. Etman, H.A. Khalil, and B.S. Azzam, "Morphology and properties of polymer matrix nanocomposites," *Int. J. Metrol. Qual. Eng.*, 1 (1) 33–39 (2010). doi:10.1051/ijmqe/2010009.
 - 39) M.S. Dresselhaus, G. Dresselhaus, R. Saito, and A. Jorio, "Raman spectroscopy of carbon nanotubes," 2005. doi:10.1016/j.physrep.2004.10.006.
 - 40) B.A.V Mikhonin, L.A. Nafie, R.K. Dukor, and S.

Issues, "Carbon nanotube characterization and quality control using portable raman : 532-nm versus 785-nm laser excitation," *Spectroscopy*, Special ed (4) 4–6 (2017).

- 41) H. Yuliani, R.D. Mayasari, E. Kalembang, Y. Deni, D.R. Santi, P.W. Pangestika, S. Purwanto, B. Sugeng, S. Suyanti, and M. Setyadji, "ANALYSIS of structure and antimicrobial activity of ceo2 and nd2o3 nanoparticles," *Spektra J. Fis. Dan Apl.*, 4 (3) 105–112 (2019). doi:10.21009/spektra.043.01.
- 42) S. Salprima Yudha, C. Banon, R. Pertiwi, D.A. Triawan, and J.I. Han, "Cost-effective synthesis of ceo2-sio2 based on oil palm leaves for the removal of toxic compounds," *Evergreen*, 10 (3) 1307–1312 (2023). doi:10.5109/7151676.
- 43) M. Kaur, N. Mittal, A. Charak, A.P. Toor, and V. Singh, "Rice husk derived activated carbon for the adsorption of scarlet rr an anionic disperse dye," *Evergreen*, 10 (1) 438–443 (2023). doi:10.5109/6782146.
- 44) N. Anantharaman, and K.M. Meera Sheriffa Begum, "Mass transfer: theory and particle," 489 387–413 (2017). <https://nitsri.ac.in/Department/Chemical Engineering/Adsorption.pdf>.
- 45) L. Pellenz, C.R.S. de Oliveira, A.H. da Silva Júnior, L.J.S. da Silva, L. da Silva, A.A. Ulson de Souza, S.M. de A.G.U. de Souza, F.H. Borba, and A. da Silva, "A comprehensive guide for characterization of adsorbent materials," *Sep. Purif. Technol.*, 305 (August 2022) (2023). doi:10.1016/j.seppur.2022.122435.
- 46) H. Pereira Neves, G. Max Dias Ferreira, G. Max Dias Ferreira, L. Rodrigues de Lemos, G. Dias Rodrigues, V. Albis Leão, and A. Barbosa Mageste, "Liquid-liquid extraction of rare earth elements using systems that are more environmentally friendly: advances, challenges and perspectives," *Sep. Purif. Technol.*, 282 (November 2021) (2022). doi:10.1016/j.seppur.2021.120064.
- 47) A. Kumari, R. Panda, M.K. Jha, J.R. Kumar, and J.Y. Lee, "Process development to recover rare earth metals from monazite mineral: a review," *Miner. Eng.*, 79 (April 2018) 102–115 (2015). doi:10.1016/j.mineng.2015.05.003.
- 48) Y. GadelHak, M. El-Azazy, M.F. Shibl, and R.K. Mahmoud, "Cost estimation of synthesis and utilization of nano-adsorbents on the laboratory and industrial scales: a detailed review," *Sci. Total Environ.*, 875 (December 2022) 162629 (2023). doi:10.1016/j.scitotenv.2023.162629.